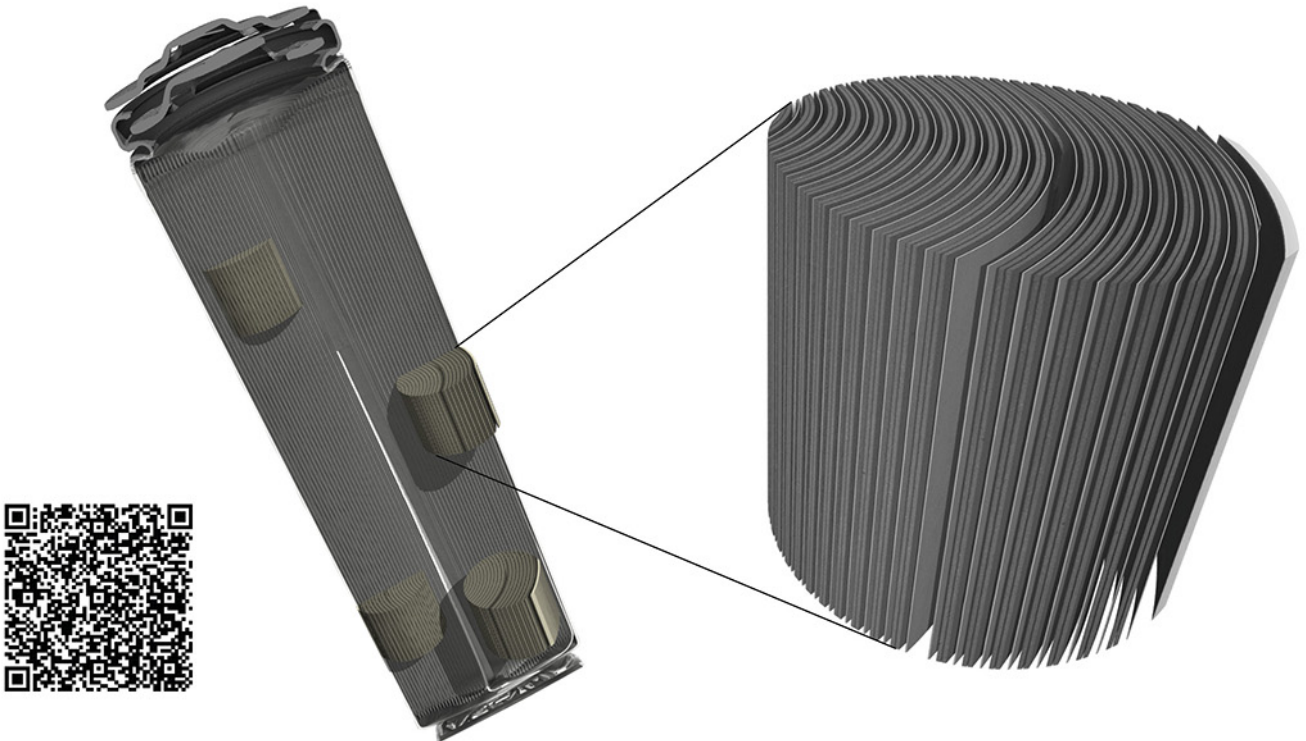


TESCAN micro-CT solutions

for energy storage materials research



TESCAN UniTOM XL

- ✓ Multi-scale non-destructive 3D imaging optimized to maximize throughput and contrast
- ✓ Fast scanning and high sample throughput with temporal resolutions below 10 seconds
- ✓ Wide array of samples types
- ✓ Enables dynamic tomography and *in-situ* experiments
- ✓ Dynamic screening for synchrotron beamtime
- ✓ Modular and open system with unmatched flexibility for research



[Click and find out more](#)

Contribution of Ferromagnetic Medium to the Output of Triboelectric Nanogenerators Derived from Maxwell's Equations

Yahui Li, Guizhong Li, Penglei Zhang, Haodong Zhang, Chao Ren, Xian Shi, Han Cai, Yanxin Zhang, Yusen Wang, Zhanfeng Guo, Hongfang Li, Guifu Ding, Haogang Cai, Zhuoqing Yang,* Chi Zhang,* and Zhong Lin Wang*

Triboelectric nanogenerators (TENGs) use the displacement current as a driving force to convert mechanical energy into electric power, which has made great contributions to micro-nano energy harvesting, self-powered systems, and the sustainable development of mankind. To date, it is accepted that the output of TENGs is only dependent on the polarization effect. This study reveals that this view is incomplete and, in reality, the magnetization effect also makes a significant contribution to the output of TENGs. For the first time, a novel insight on the output of TENGs is discovered through the theoretical derivation and analysis of Maxwell's equations in ferromagnetic medium. Experimentally, TENGs based on ferromagnetic media are constructed, which exhibit higher output than that of non-ferromagnetic media based. Interestingly, the output behavior of ferromagnetic media based TENGs is strongly related to the external magnetic field ambient, which is well demonstrated. The discovered output characteristics of TENGs are precisely derived from the working principle of TENGs, simultaneously, a completed and unified theoretical system is constructed for TENGs. This significant discovery and theory will be an indispensable supplement to the existing research on TENGs and also provide a general guidance and deeper understanding of the TENG.

1. Introduction

To alleviate the increasingly severe energy situation and satisfy the self-powered systems, it is critical to explore sustainable and micro-nano energy that could both satisfy the social development and resolve the global energy crisis.^[1–3] In particular, harvesting energy from nature, such as the sunlight, wind, ocean, mechanical motion, etc., is considered as a strategic way for enabling the energy security.^[4–9] Ever since the discovery of triboelectric nanogenerators (TENGs) in 2012, researchers have been inspired by the idea of using the charging process in triboelectric layer to convert mechanical energy into electric power.^[10] Their shared dream is to collect mechanical energy widely present in the surrounding environment and people's daily life and convert them into electrical energy.^[11–13] TENGs, working under the principle of contact electrification and electrostatic induction, have been

Dr. Y. H. Li, P. L. Zhang, Dr. H. D. Zhang, C. Ren, Dr. X. Shi, Dr. H. Cai, Dr. Y. X. Zhang, Dr. Y. S. Wang, Z. F. Guo, Dr. H. F. Li, Prof. G. F. Ding, Prof. Z. Q. Yang


National Key Laboratory of Science and Technology on Micro/Nano Fabrication
Shanghai Jiao Tong University
Shanghai 200240, China
E-mail: yzhuoqing@sjtu.edu.cn

Dr. Y. H. Li, P. L. Zhang, Dr. H. D. Zhang, C. Ren, Dr. X. Shi, Dr. H. Cai, Dr. Y. X. Zhang, Dr. Y. S. Wang, Z. F. Guo, Dr. H. F. Li

Department of Micro/Nano Electronics
School of Electronic Information and Electrical Engineering
Shanghai Jiao Tong University
Shanghai 200240, China

Dr. G. Z. Li

Shenzhen Key Laboratory for Advanced Materials
Harbin Institute of Technology
Shenzhen 518055, China

 The ORCID identification number(s) for the author(s) of this article can be found under <https://doi.org/10.1002/aenm.202003921>.

Prof. H. G. Cai

Tech4Health Institute and Department of Radiology
NYU Langone Health
New York, NY 10016, USA

Prof. C. Zhang, Prof. Z. L. Wang

CAS Center for Excellence in Nanoscience
Beijing Key Laboratory of Micro-nano Energy and Sensor
Beijing Institute of Nanoenergy and Nanosystems
Chinese Academy of Sciences
Beijing 100083, China

E-mail: czhang@binn.cas.cn; zlwang@gatech.edu

Prof. C. Zhang, Prof. Z. L. Wang
School of Nanoscience and Technology
University of Chinese Academy of Sciences
Beijing 100049, China

Prof. Z. L. Wang
School of Material Science and Engineering
Georgia Institute of Technology
Atlanta, GA 30332-0245, USA

DOI: 10.1002/aenm.202003921

demonstrated by previously reported works.^[14–16] Specifically, the contact electrification determines the transferred and stored charges in the triboelectric layer, and the electrostatic induction determines the amount of charges that can be induced and exported.

Typically, TENG uses the displacement current as a driving force to effectively convert mechanical energy into electric power, which is an extended application of Maxwell's equations in the field of nano energy.^[17] However, the displacement current that could be generated by magnetic materials is almost overlooked in TENG. Historically, the displacement current was introduced into Ampere's law for satisfying the continuity equations of the charges, and it was also proved by Maxwell that electricity and magnetism are equivalent.^[17,18] On one hand, an electrical current could push the movement of magnetic domain by the coupling interaction between conduction electrons and localized magnetic moments, which was well studied.^[19–22] On the other hand, an electromotive force generated by the movement and reorganization of magnetic domain wall was also predicted and demonstrated.^[23–27] According to the fourth term of Maxwell's equations (circuital law with Maxwell's addition), the changing electric flux can generate a magnetic field, which can magnetize the magnetic medium, resulting in magnetization.^[17] Similar to the alternating current generated by TENG in the periodic contact-separation movement, a magnetic field is also generated around the device. Therefore, a magnetizing current and an electric field will be generated theoretically if a magnetic medium is introduced into TENG, which will improve TENG's electrical output and the energy conversion efficiency.

In ferromagnetic substances, there is a powerful molecular field, which is originated from the mutual interaction between electrons. In addition, the magnetic moments of a specific area tend to be ordered, resulting in saturated magnetization in such a local area, which is also referred as magnetic domain.^[28,29] However, owing to the irregular thermal motion, the magnetization direction of each domain is randomly arranged, and the magnetic moments among these magnetic domains mutually offset each other. Therefore, the entire macro-ferromagnet does not exhibit magnetization without an external magnetic field.^[30] Once driven by an external magnetic field, the magnetic moments tend to align with the external field, thus forming an additional magnetic field and generating magnetizing current in this dynamic process.^[28,31,32] Therefore, we propose to couple a magnetic field generated by the displacement current with the ferromagnetic medium for improving the output characteristics of TENG.

Based on the model of single electrode triboelectric nanogenerators (S-TENG), here we demonstrate that using ferromagnetic electrodes could improve TENG's performance, including short-circuit current, open-circuit voltage, transferred charges, and power density. This enhancement is originated from the Maxwell's equations and does not involve any additional design or fabrication process, such as materials modification, patterned structure, or structure optimization. Through the derivation and simulation of a physical model, the performance of TENG was predicted theoretically and then verified experimentally. Furthermore, the dynamic micro simulation and in situ information of domain wall structures in ferromagnetic

electrode during magnetization were also investigated, which further confirm this proposed mechanism from a microscopic point of view. Anyway, the novel mechanism for enhancing TENG's performance proposed in this work is precisely originated from the working principle of TENG, which will provide a deep understanding of the theoretical mechanism for triboelectric devices and bring meaningful guidance for the future development and optimization of TENG.

2. Results and Discussion

2.1. Theoretical Prediction of TENG Output Based on Maxwell's Equations

Based on the contact electrification and the principle of TENG, original Maxwell's equations [Equations (1.1)–(1.4)] can be used to predict and derive the output of TENG as follows^[33,34]

$$\nabla \cdot \mathbf{D} = \rho \quad (1.1)$$

$$\nabla \cdot \mathbf{B} = 0 \quad (1.2)$$

$$\nabla \times \mathbf{E} = -\frac{\partial \mathbf{B}}{\partial t} \quad (1.3)$$

$$\nabla \times \mathbf{H} = \mathbf{J} + \frac{\partial \mathbf{D}}{\partial t} \quad (1.4)$$

where \mathbf{D} is the electric displacement vector, and $\mathbf{D} = \epsilon_0 \mathbf{E} + \mathbf{P}$. Practically, in addition to the polarization caused by electric field, there also exists polarization induced by nonelectric field, such as piezoelectric and triboelectric effect. Therefore, an additional term of \mathbf{P}_s is added in \mathbf{D} for explaining the contribution of electrostatic charges induced by contact electrification as follows

$$\mathbf{D} = \epsilon_0 \mathbf{E} + \mathbf{P} + \mathbf{P}_s \quad (2.1)$$

$$\mathbf{D}' = \epsilon_0 \mathbf{E} + \mathbf{P} \quad (2.2)$$

$$\mathbf{D} = \mathbf{D}' + \mathbf{P}_s \quad (2.3)$$

where \mathbf{D}' in Equation (2.2) is the electric displacement vector induced by electrical field. Therefore, the Maxwell's equations in TENG can be written as follows^[33,35]

$$\nabla \cdot \mathbf{D}' = \rho - \nabla \cdot \mathbf{P}_s \quad (3.1)$$

$$\nabla \cdot \mathbf{B} = 0 \quad (3.2)$$

$$\nabla \times \mathbf{E} = -\frac{\partial \mathbf{B}}{\partial t} \quad (3.3)$$

$$\nabla \times \mathbf{H} = \mathbf{J} + \frac{\partial \mathbf{D}'}{\partial t} + \frac{\partial \mathbf{P}_s}{\partial t} \quad (3.4)$$

Note that ρ in Equation (3.1) is the distribution of total charges in space, including free charges and polarization

charges. In Equation (3.4), the first term J is the density of free conduction current in space as a result of flowing charges; the second term $\frac{\partial D'}{\partial t}$ is the displacement current induced by electric field; and the third term $\frac{\partial P_s}{\partial t}$ is the displacement current induced by nonelectric field.

For ferromagnetic media, we have

$$D' = \epsilon_0 E + P = \epsilon E \quad (4.1)$$

$$B = \mu_0 (H + M) = \mu(H)H \quad (4.2)$$

where ϵ_0 , ϵ , μ_0 , $\mu(H)H$, and M are the vacuum dielectric constant, dielectric constant, vacuum permeability, ferromagnetic permeability, and magnetization, respectively. Especially, the ferromagnetic permeability ($\mu(H)H$) for ferromagnetic media is dependent on the varying magnetic field.

Start from Equation (4.2), which can be deformed as follows

$$\nabla \times B = \mu_0 \nabla \times H + \mu_0 \nabla \times M \quad (5.1)$$

By substituting Equation (3.4) into Equation (5.1), we have

$$\nabla \times B = \mu_0 J + \mu_0 \frac{\partial D'}{\partial t} + \mu_0 \left(\frac{\partial P_s}{\partial t} + \nabla \times M \right) \quad (5.2)$$

where the terms related to the output of TENG can be expressed as follows

$$J_{\text{TENG}} = \frac{\partial P_s}{\partial t} + \nabla \times M \quad (5.3)$$

That is, both the polarization induced by nonelectric field and the magnetization field could contribute to the displacement current of TENG and the output. According to Equation (5.3) derived above, the output of TENG is related to the M . For non-ferromagnetic media, they do not respond to the magnetic fields, therefore, the term of $\nabla \times M$ is zero. While for ferromagnetic media, the initial permeability is an indicator of the magnetization intensity for a magnetic medium. Based on the relationship between M and μ described in Equation (4.2), the greater the permeability, the greater the magnetization intensity (M), therefore, the larger output of TENG.

For ferromagnetic materials, there are many magnetic domains inside and shows spontaneous magnetization (Figure 1a). The source of spontaneous magnetization is the electron spin magnetic moment, that is, there is a state in which the electron shell of an atom is not filled with electrons. According to the principle of minimum energy, Pauli's exclusion principle, and Hund's rules,^[36,37] the arrangement of electrons outside the nucleus of common ferromagnetic substances is shown in Figure S1 (Supporting Information). Specifically, the 3d orbits of iron, cobalt, and nickel have four, three, and two vacancies, respectively, which is the source of electron spin magnetic moment. Additionally, according to the bonding theory, the energy in 3d and 4s orbit of a transition metal atom is not much different (Fe, Co, Ni), therefore, their electron clouds could be overlapped and cause the redistribution of electrons in 3d and 4s states (Figure 1b,c). Such an

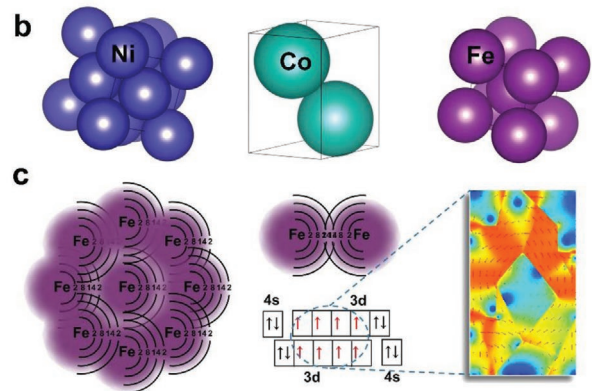
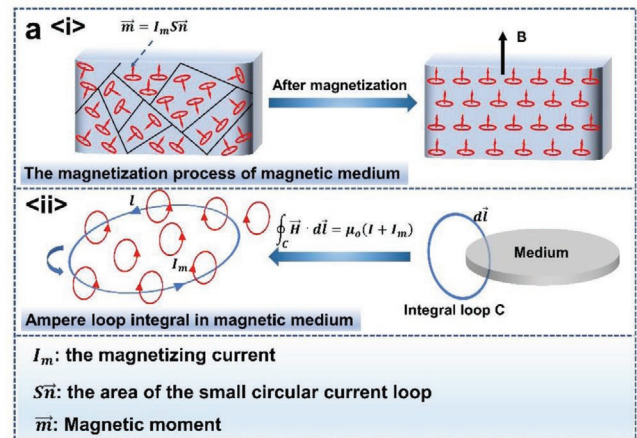


Figure 1. The mechanism analysis of ferromagnetic medium enhanced output of triboelectric nanogenerator derived from Maxwell's equations. a) Schematic diagram of magnetization process and the Ampere's loop law of magnetic medium. b) Schematic diagram of the crystal structure of iron, cobalt, and nickel. c) Schematic diagram of the electron clouds of iron atoms, the overlapping of electron clouds outside the nucleus, and the formation of magnetic domains.

exchange interaction (exchange integral A) generates a kind of exchange energy, and the magnetic moments of adjacent atoms are aligned in the same direction when the exchange integral is positive ($A > 0$), thereby achieving spontaneous magnetization. Besides, the exchange integral A is strongly dependent on the distance between the nuclei, i.e., the lattice constant. Only when the ratio of the distance between the atomic nuclei and the radius of electron shell participating in exchange is greater than 3, the exchange integral is positive. Therefore, iron, cobalt, and nickel satisfy the requirements for spontaneous magnetization at room temperature.^[29,31] Based on the theoretical analysis and physical laws, ferromagnetic inducing electrodes will not only provide the characteristics of conductors for electrostatic induction but also improve the performance of TENG by increasing the displacement current.

2.2. TENG Working Principle and Electrostatic Simulation

Similar to the conventional TENG,^[33,34] the working principle of S-TENG to convert mechanical energy into electrical power involves contact electrification and electrostatic induction

(Figure S2a, Supporting Information). The corresponding electrostatic simulation is illustrated in Figure S2b (Supporting Information). In this work, poly-dimethylsiloxane (PDMS) was used as a negative triboelectric layer for contacting with skin and harvesting energy considering its high electronegativity and biocompatibility.^[38] Typically, when finger and PDMS are in physical contact, the electrons will be transferred from finger to PDMS owing to the differences in triboelectric series, resulting in an equal amount and opposite polarity charges on the interface of finger and PDMS, respectively. Meanwhile, the negative charges stored in PDMS could be kept for a certain period owing to the insulated characteristics of polymer layer (Figure S2ai, Supporting Information), and there is no output voltage at this stage from the simulated results (Figure S2bi, Supporting Information). Subsequently, as the finger starts to release, opposite charges on the surface of finger and PDMS are separated from each other and could not be completely neutralized owing to the presence of an air layer. To reach electrostatic equilibrium, the electrode on the back correspondingly induces a certain amount of positive charges that are opposite to the un-neutralized charges on PDMS. Thus, a potential difference between the electrode and ground is established, driving electrons from the electrode to ground through an external circuit and generating an electrical output signal (Figure S2aii,bii, Supporting Information). Then, when it reaches to a certain distance between finger and PDMS, which are completely separated from each other, the charges induced by electrode are saturated and the output voltage of TENG reaches the highest at this moment (Figure S2aiii,biii, Supporting Information). Afterward, when the finger and PDMS are gradually approaching, the separated distance decreases. The positive charges on finger could neutralize a portion of negative charges on the PDMS, which makes the positive charges on the inducing electrode decrease. Meanwhile, the electrons are flowing from ground to the inducing electrode through an external circuit, reducing the surface's potential of the inducing electrode (Figure S2aiv,biv, Supporting Information). Finally, once the physical contact is restored again between the finger and PDMS, the opposite charges supported by them could neutralize each other. There is no induced charges in the electrode, and consequently, there are neither voltage nor current signals. The potentials of electrode at different distances between the finger and PDMS are simulated, as shown in Figure S2c (Supporting Information). The relationships between electrical characteristics and separation distance are plotted in Figure S2d,e (Supporting Information). As the separated distance increases, the surface potential of inducing electrode and the amount of transferred charges gradually increases and finally reaches a stabilized status. The measured electrical signals of S-TENG during the periodic contact-separation movement, including short-circuit, open-circuit voltages, and transferred charges, are presented in Figure S2f-h (Supporting Information), which are consistent with the working model discussed in Figure S2a (Supporting Information).

2.3. Improved Output of TENG with Ferromagnetic Media

In this work, the electrical and magnetic characteristics of various electrodes were simulated and calculated. Based on

the principle of TENG, the simulation model simultaneously involves both electricity and magnetism. The circuit diagram of electromagnetic simulation is shown in Figure S3a (Supporting Information). Figure S3b-e (Supporting Information) shows the input alternating current (AC), conductivity, and relative permeability in the electromagnetic simulation. It can be clearly seen from the simulated diagram (Figure S3f and Note S1, Supporting Information) that the magnetic line density of ferromagnetic electrodes (iron, nickel, cobalt) increases significantly compared with that of traditional electrodes (silver, copper, aluminum). The simulated magnetic flux density under AC excitation increases with increasing the magnetic permeability of electrodes (Figure S3g, Supporting Information). There is no obvious difference in magnetic flux density among traditional conductive electrodes (Figure S3h, Supporting Information). The average magnetic flux density increases by three orders of magnitude from 10^{-11} T for traditional electrodes to 10^{-8} T for ferromagnetic electrodes (Figure S3i, Supporting Information). The increased magnetic flux density shows that the magnetization current is accompanied by the magnetization process in ferromagnetic electrodes, which makes additional contribution to the improvement of TENG's performance.

The conductivity of a thin film is closely related to its thickness, i.e., the square resistance (R_s) generally decreases with an increasing thickness. For better comparison, various electrodes used in this work have the same thickness of about $50 \mu\text{m}$. Figure 2a shows the cross-section scanning electron microscopy (SEM) images and elemental mappings of TENG with various electrodes, showing the layered structure of inducing electrode/PDMS, and confirming the electrode composition. In addition, the composition and elemental distribution of the negative triboelectric layer PDMS used in various TENG were also confirmed, which mainly includes silicon, carbon, and oxygen (Figure S4, Supporting Information). Furthermore, SEM was performed to examine the surface topography of inducing electrodes. Despite the differences in surface morphology, in general, all surfaces are flat without any prominent micro/nanostructures (Figure S5, Supporting Information). Figure S6 (Supporting Information) shows the X-ray diffraction (XRD) spectra of individual electrodes, further confirming the crystal structures of various metallic electrodes. Figure 2b-d shows the short-circuit current density, open-circuit voltage, and transferred charges of different TENG based on traditional electrodes (Ag, Cu, Al) and ferromagnetic electrodes (Fe, Ni, Co). Figure 2e-g shows the comparison of peak electrical signals of TENG based on different electrodes. Overall, the output characteristics of TENG based on traditional electrodes are lower and virtually the same, while those of ferromagnetic electrodes are much higher. Figure 2h shows the comparison of square resistance, which are much smaller for traditional conductive electrodes than ferromagnetic electrodes. Nevertheless, the instantaneous ideal power density of TENG supported by ferromagnetic electrodes is significantly higher than that of traditional electrodes (Figure 2i and Note S2, Supporting Information). The power density of Fe-based TENG is about twice of traditional ones, and the power density of Ni, Co-based TENG is about 1.5-folds of traditional ones. In general, the initial permeability is a key indicator of the magnetic sensitivity. For ferromagnetic electrodes used in this work, the initial relative

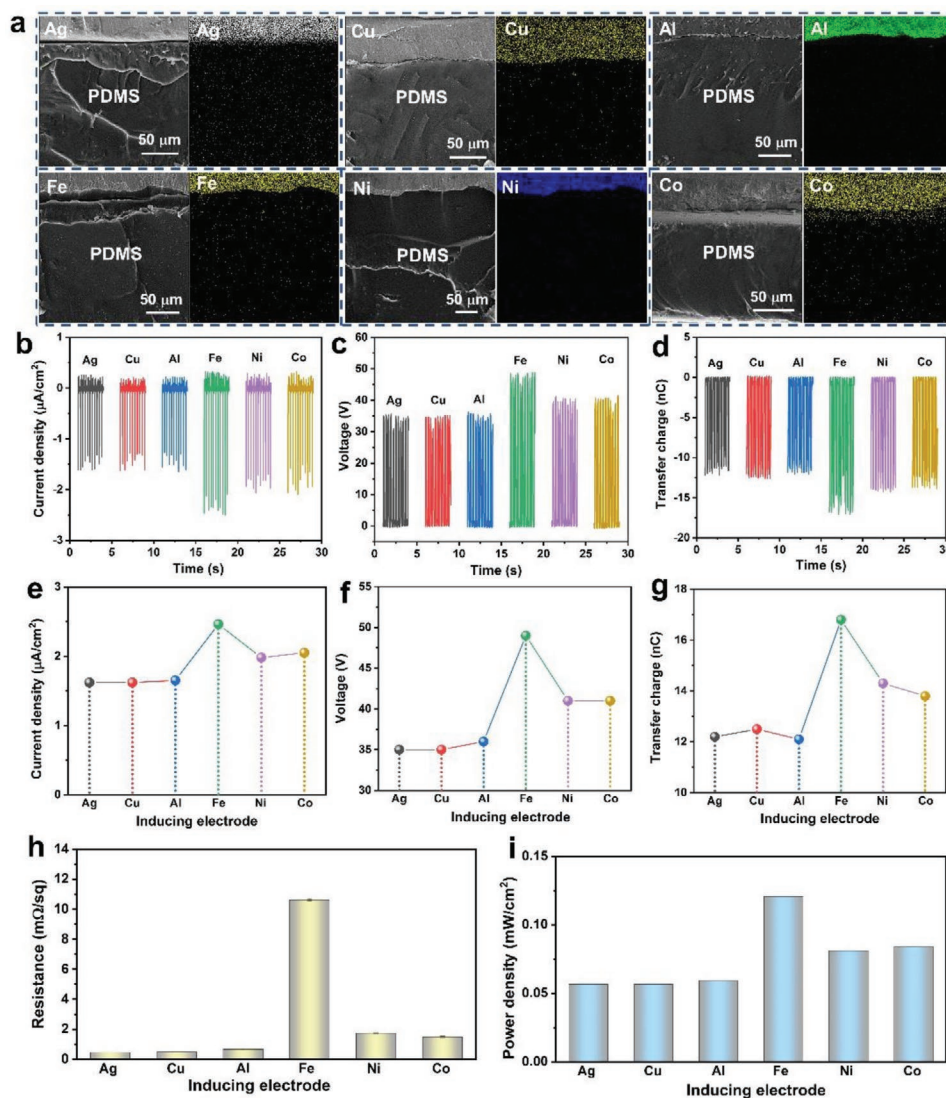


Figure 2. The structure and output of the fabricated TENG supported by different electrodes. a) The cross-section SEM images and elemental mappings of different TENG. b–d) The short-circuit current density, open-circuit voltage, and transferred charges of different TENG. e–g) The comparison of short-circuit current density, open-circuit voltage, and the transferred charges among different TENG. h) The square resistance of different inducing electrodes. i) The comparison of instantaneous ideal power density among different TENG.

permeability of Fe is larger than that of Ni and Co, and the latter two are close to each other (Figure S7, Supporting Information). As a result, the TENG with Fe electrode has the best electrical performance, TENG with Ni and Co electrodes have equivalent performance lower than Fe, but higher than traditional electrodes. The experimental results are consistent with theoretical and simulation expectations. As long as a certain conductivity is satisfied, increasing the magnetic permeability of inducing electrodes could significantly enhance the output characteristics of TENG.

To investigate the influence of electrode thickness on the output of TENG, in detail, we choose two typical materials, Cu versus Ni, as inducing electrode with different thickness for the fabrication of TENG. For Cu-based TENG, the electrode thickness varies among 10, 20, 30, 50, and 100 μm. Figure S8a–c (Supporting Information) shows the short-circuit current

density, open-circuit voltage, and transferred charges of Cu-based TENG with different electrode thickness. Figure S8d (Supporting Information) shows the square resistance of electrodes at different thickness. The square resistance decreases significantly with increasing thickness, indicating that the conductivity of electrodes is significantly improved. However, there is no significant difference in the electrical performance and power density of TENG based on different thickness electrode, as summarized in Figure S8e,f (Supporting Information). Similarly, for the Ni-based TENG, the short-circuit current density, open-circuit voltage, and transferred charges are almost identical for different electrode thickness (Figure S8g–i, Supporting Information). The square resistance of Ni electrodes decreases with increasing thickness, but the output of TENG is independent on thickness (Figure S8j–l, Supporting Information). The nondependent conclusions of thickness on TENG's

performance based on this work are consistent with the previously reported.^[39] Notably, despite a lower conductivity of Ni electrode than that of Cu electrode with the same thickness, the output characteristics of Ni-based TENG are better than Cu, revealing the magnetizing current generated by Ni electrode makes significant contribution to the output of TENG.

To further verify the proposed mechanism, the Cu- and Ni-based TENG were examined under different magnetic field environments. Figure 3a is the schematic diagram of

skin-based S-TENG and the contact-separation movement between finger and PDMS. Figure 3b is the testing schematic of S-TENG at different magnetic field angles, which varied from 0° to 180° (under a constant strength of 500 Gs). Figure 3c is the testing schematic of S-TENG under different magnetic field strength, which was varied among 0, 500 and 2000 Gs, respectively (at a constant angle of 0°). For Cu-based TENG, the output is basically the same with the varying magnetic field angles, indicating that the traditional electrode has no

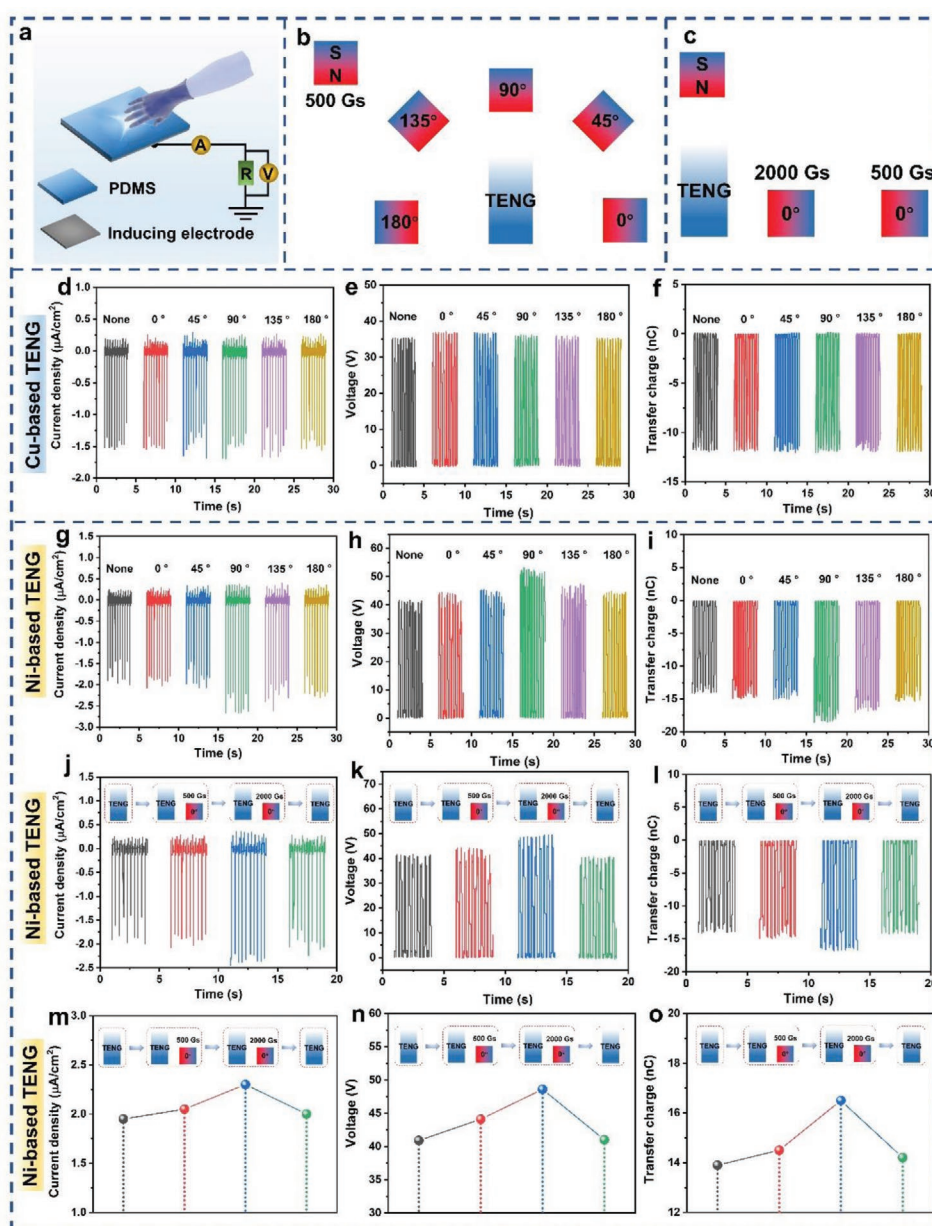


Figure 3. The output of TENG under an external magnetic field. a) Schematic diagram of skin-based single triboelectric nanogenerator and the contact-separation movement between finger and PDMS. b) The testing schematic of S-TENG under different magnetic field angles with 500 Gs. c) The testing schematic of S-TENG under different magnetic field strength (0-500-2000-0 Gs). d-f) The short-circuit current density, open-circuit voltage, and transferred charges of Cu-based TENG under different magnetic field angles. g-i) The short-circuit current density, open-circuit voltage, and transferred charges of Ni-based TENG under different magnetic field angles. j-l) The short-circuit current density, open-circuit voltage, and transferred charges of Ni-based TENG under different magnetic field strength (0-500-2000-0 Gs). m-o) The comparison of short-circuit current density, open-circuit voltage, and transferred charges of Ni-based TENG under different magnetic field strength (0-500-2000-0 Gs).

obvious response to the external magnetic field and only plays a role of charge conduction and separation in the electrostatic induction process (Figure 3d–f). While for Ni-based TENG, the short-circuit current density, open-circuit voltage, and transferred charges change significantly with the varying magnetic field angles (Figure 3g–i). Notably, the output of TENG is enhanced prominently after applying an external magnetic field, and the maximum output is reached at the angle of 90°. According to Equation (5.3), the term $\nabla \times \mathbf{M}$ is a vector that is orientation-dependent. The magnetization effect of ferromagnetic electrodes inside the TENG depends on the external magnetic field angle. Therefore, the output of TENG varies with the magnetic field angles during mechanical triggering. Additionally, the output of TENG was investigated under the same angle (0°) with different strength, which was controlled by adjusting the distance between the magnet and TENG. Figure 3j–l shows the short-circuit current density, open-circuit voltage, and transferred charges of Ni-based TENG under different magnetic field strength, indicating the output of TENG is improved by increasing the magnetic field strength at a constant angle of 0°. After the examination at 2000 Gs, the TENG's performance was retested under the condition without an external magnetic field, and the output was much lower (Figure 3m–o). The magnetization effect on the internal magnetic domain structure is different for different magnetic field strengths ($\nabla \times \mathbf{M}$), resulting in different output of TENG. Compared with the initial output of TENG without a magnetic field, the retested performance under no magnetic field had a slight increment, which is probably caused by the remanence inside the ferromagnetic

electrode under the action of a strong magnetic field. Overall, the output behavior of TENG based on ferromagnetic electrode is strongly related to the external magnetic field environment, further matching the Maxwell's equations theory and verifying the proposed enhancement mechanism.

2.4. Microscopic Simulation and In Situ Observation of Magnetization and Domain Structure

Figure 4a shows the simulated evolution of magnetic domains inside a ferromagnetic electrode, which is under the action of an external magnetic field. Before applying the magnetic field, the total magnetic moment exhibited externally is approximately zero, but the magnetic moment of individual domain is distinct from each other, with nonzero strength (Figure 4ai). Subsequently, the variable magnetic flux density is increased under the action of an external magnetic field. Meanwhile, the magnetic moment's direction of partial magnetic domains tends to align with the external magnetic field, resulting in a nonzero total magnetic moment and improved magnetic field strength (Figure 4aai). Finally, more and more magnetic domains align with the applied magnetic field and reach the saturated state. Meanwhile, the magnetic flux density and magnetic field intensity displayed externally reach the largest values (Figure 4aaii). Figure 4b,c presents the in situ observation of magnetic domains by Lorentz-transmission electron microscope, revealing the structure of magnetic domains and the direction of magnetic domain walls with and without

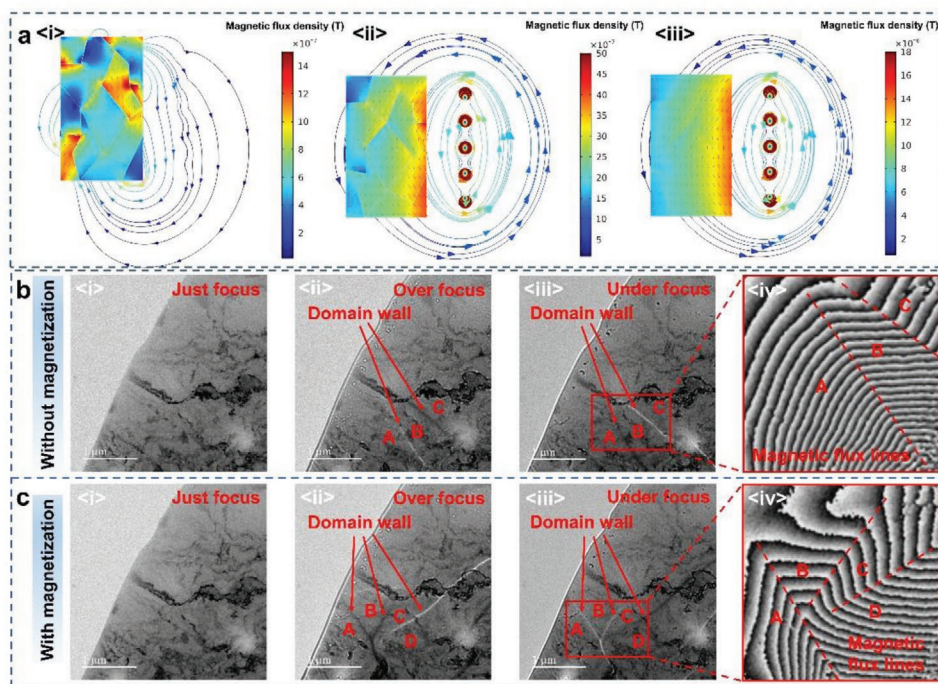


Figure 4. Microscopic simulation and in situ observation of magnetization and domain structures. a) The simulation of magnetic flux density corresponding to the initial magnetization, intermediate magnetization, and saturated magnetization. b) The structure and magnetic flux lines of magnetic domains without magnetization based on iron: i) just focus; ii) over focus; iii) under focus; and iv) the enlarged image of magnetic domains and domain walls. c) The structure and magnetic flux lines of magnetic domains with magnetization based on iron: i) just focus; ii) over focus; iii) under focus; and iv) the enlarged image of magnetic domains and domain walls.

magnetization. The magnetic domain walls could be clearly identified by comparing the under-focused and over-focused images, and the magnetic flux lines in the corresponding area could also be observed via the electronic holography. The in situ characterization during the magnetization process further demonstrates that the microstructures of magnetic domains have changed significantly, accompanied by the deflection and movement of the magnetic domain walls (Figure 4biv,civ). As a result, the movement of magnetic domain walls and the changes of domain structures lead to the changes of spatial magnetic field and the formation of displacement electric field.

3. Conclusion

In summary, we have predicted and proposed a novel effect of spatially varying magnetic field on the displacement current of triboelectric nanogenerators, where is starting from the Maxwell's equations, and the output characteristics of TENG is redefined and explained. To our best knowledge, this discovery and theory is proposed for the first time since the creation of triboelectric nanogenerator. We found that not only the polarization effect, but the magnetization effect can also make great contributions to the output of TENG. Experimentally, TENGs based on ferromagnetic media are constructed, which exhibit higher output than that of non-ferromagnetic media based. Interestingly, we found that the TENG output behaviors are closely related to the external magnetic field ambient, further verifying our proposed theoretical analysis and systems for TENG. Finally, we believe that this interesting and significant discovery will be an indispensable supplement to the existing research of TENG, and a completed and unified theoretical system is also constructed for TENG, which will provide a deep understanding of the theoretical mechanism for triboelectric devices and bring meaningful guidance for the future development and optimization of TENG.

4. Experimental Section

Fabrication and Measurements of the S-TENG Supported by Different Electrodes: The thickness of inducing electrodes used in this work was controlled at about 50 μm , and its morphology and structural characterization were carried out by SEM and XRD. Then the electrodes with a diameter of 3 in. were fixed on glass substrate with the same size, and the spin-coating of PDMS (Sylgard 184 silicone elastomer) was conducted, i.e., PDMS/electrode/glass. Afterward, the samples were placed on a hot plate for curing at 120 $^{\circ}\text{C}$ (details in Note S3, Supporting Information). Finally, the S-TENG supported by various electrodes were cut to the same size ($2 \times 1 \text{ cm}^2$) for examining the electrical output. The short-circuit current, open-circuit voltage, and transferred charges were examined through a Keithley 6514 electrometer. In the process of testing, all samples would continuously accumulate charges during the periodic contact-separation movements until a stable output signal was reached, as shown in Figure S9 (Supporting Information). In addition, the test details and results of the contact-separation TENG based on a dual-electrode mode ($2 \times 2 \text{ cm}^2$) have been presented in Note S4, Figures S10 and S11 (Supporting Information).^[40,41]

TENG's Electromagnetic Simulation and Analysis: The working principle of TENG was simulated by using an electrostatic field model. The ferromagnetic electrodes used in TENG were simulated via electromagnetic field, and its mechanism was analyzed from

the perspective of microscopic magnetic domains. Except that the electrostatic simulation is a stable state physical field, the rest are simulated in a transient physical field.

Fundamental Characterization and Analysis: The topography of electrodes was analyzed by a JEOL JSM-7800F field-emission scanning electron microscope (JEOL, Japan), indicating the flat electrode surface without any microstructures. The layered structure and chemical composition of the fabricated S-TENGs were observed by an energy-dispersion spectrum (EDS) and elemental surface scanning. The phase structure of various electrodes was characterized by a D/max 2500PC high-resolution X-ray diffractometer (Rigaku, Japan) with $K\alpha$ radiation, proving the crystal plane structure of the electrodes. The magnetic performance of ferromagnetic electrodes was obtained by a SQUID vibrating sample magnetometer (VSM), including the initial permeability (Quantum Design, USA). Additionally, the in situ observation of magnetic domains structure and domain walls was performed by a JEM-2100F Lorentz-transmission electron microscope (JEOL, Japan), which reveals the dynamic changes during the magnetization.

Supporting Information

Supporting Information is available from the Wiley Online Library or from the author.

Acknowledgements

This work was supported in part by the National Key Research and Development Program of China (2020YFB2008503), the National Natural Science Foundation of China (No. 61974088), and the Advanced Research Ministry of Education Joint Foundation (6141A02022424). The authors would like to thank instrumental analysis center of Shanghai Jiao Tong University (SJTU) for the experimental support (JEOL JSM-7800F), as well as Zhongqiu Bao for the scanning electron microscope analysis. The authors also thank the Guangzhou Puchuan Testing Technology Co., Ltd. for vibrating sample magnetometer measurements.

Conflict of Interest

The authors declare no conflict of interest.

Data Availability Statement

The data that support the findings of this study are available from the corresponding author upon reasonable request.

Keywords

ferromagnetic medium, magnetization effect, Maxwell's equations, triboelectric nanogenerators

Received: December 20, 2020

Revised: March 4, 2021

Published online:

[1] L. Gu, J. Liu, N. Cui, Q. Xu, T. Du, L. Zhang, Z. Wang, C. Long, Y. Qin, *Nat. Commun.* **2020**, *11*, 1030.

[2] Z. L. Wang, J. Song, *Science* **2006**, *312*, 242.

- [3] Y. Jie, Q. Jiang, Y. Zhang, N. Wang, X. Cao, *Nano Energy* **2016**, *27*, 554.
- [4] M. Grätzel, *Nature* **2001**, *414*, 338.
- [5] G. Zhu, Y. Su, P. Bai, J. Chen, Q. Jing, W. Yang, Z. L. Wang, *ACS Nano* **2014**, *8*, 6031.
- [6] Y. Guo, Y. Chen, J. Ma, H. Zhu, X. Cao, N. Wang, Z. L. Wang, *Nano Energy* **2019**, *60*, 641.
- [7] W. Song, X. Yin, D. Liu, W. Ma, M. Zhang, X. Li, P. Cheng, C. Zhang, J. Wang, Z. L. Wang, *Nano Energy* **2019**, *65*, 103997.
- [8] X. Wang, J. Song, J. Liu, Z. L. Wang, *Science* **2007**, *316*, 102.
- [9] X. Cao, Y. Jie, N. Wang, Z. L. Wang, *Adv. Energy Mater.* **2016**, *6*, 1600665.
- [10] F. R. Fan, Z. Q. Tian, Z. L. Wang, *Nano Energy* **2012**, *1*, 328.
- [11] Y. Jie, X. Jia, J. Zou, Y. Chen, N. Wang, Z. L. Wang, X. Cao, *Adv. Energy Mater.* **2018**, *8*, 1703133.
- [12] J. Chen, Y. Huang, N. Zhang, H. Zou, R. Liu, C. Tao, X. Fan, Z. L. Wang, *Nat. Energy* **2016**, *1*, 328.
- [13] Y. Yang, H. Zhang, J. Chen, Q. Jing, Y. S. Zhou, X. Wen, Z. L. Wang, *ACS Nano* **2013**, *7*, 7342.
- [14] J. Liu, A. Goswami, K. Jiang, F. Khan, S. Kim, R. McGee, Z. Li, Z. Hu, J. Lee, T. Thundat, *Nat. Nanotechnol.* **2018**, *13*, 112.
- [15] J. Liu, M. Miao, K. Jiang, F. Khan, A. Goswami, R. McGee, Z. Li, L. Nguyen, Z. Hu, J. Lee, *Nano Energy* **2018**, *48*, 320.
- [16] J. Liu, Y. Zhang, J. Chen, R. Bao, K. Jiang, F. Khan, A. Goswami, Z. Li, F. Liu, K. Feng, *Matter* **2019**, *1*, 650.
- [17] Z. L. Wang, *Mater. Today* **2017**, *20*, 74.
- [18] N. L. Schryer, L. R. Walker, *J. Appl. Phys.* **1974**, *45*, P.5406.
- [19] M. Kläui, P.-O. Jubert, R. Allenspach, A. Bischof, J. A. C. Bland, G. Faini, U. Rüdiger, C. A. Vaz, L. Vila, C. Vouille, *Phys. Rev. Lett.* **2005**, *95*, 026601.
- [20] A. Yamaguchi, T. Ono, S. Nasu, K. Miyake, K. Mibu, T. Shinjo, *Phys. Rev. Lett.* **2004**, *92*, 077205.
- [21] G. S. D. Beach, C. Knutson, C. Nistor, M. Tsoi, J. L. Erskine, *Phys. Rev. Lett.* **2006**, *97*, 057203.
- [22] M. Hayashi, L. Thomas, Y. B. Bazaliy, C. Rettner, R. Moriya, X. Jiang, S. S. P. Parkin, *Phys. Rev. Lett.* **2006**, *96*, 197207.
- [23] L. Berger, *Phys. Rev. B* **1986**, *33*, 1572.
- [24] S. E. Barnes, S. Maekawa, *Phys. Rev. Lett.* **2007**, *98*, 246601.
- [25] A. R. Duine, *Phys. Rev. B* **2008**, *77*, 014409.
- [26] W. M. Saslow, *Phys. Rev. B: Condens. Matter Mater. Phys.* **2007**, *76*, 184434.
- [27] S. A. Yang, G. S. Beach, C. Knutson, D. Xiao, Q. Niu, M. Tsoi, J. L. Erskine, *Phys. Rev. Lett.* **2009**, *102*, 067201.
- [28] J. H. Van Vleck, *Rev. Mod. Phys.* **1945**, *17*, 27.
- [29] C. Kittel, *Phys. Rev.* **1946**, *70*, 965.
- [30] C. S. Edmund, *Rep. Prog. Phys.* **2002**, *13*, 83.
- [31] C. Kittel, *Rev. Mod. Phys.* **1949**, *21*, 541.
- [32] H. J. Williams, W. Shockley, *Phys. Rev.* **1949**, *75*, 178.
- [33] Z. L. Wang, *Nano Energy* **2020**, *68*, 104272.
- [34] Z. L. Wang, A. C. Wang, *Mater. Today* **2019**, *30*, 34.
- [35] F. Wilczek, *Phys. Rev. Lett.* **1982**, *48*, 1144.
- [36] E. U. Condon, J. E. Mack, *Phys. Rev.* **1930**, *35*, 579.
- [37] J. Katriel, R. Pauncz, *Adv. Quantum Chem.* **1977**, *10*, 143.
- [38] G. Z. Li, G. G. Wang, D. M. Ye, X. W. Zhang, Z. Q. Lin, H. L. Zhou, F. Li, B. L. Wang, J. C. Han, *Adv. Electron. Mater.* **2019**, *5*, 1800846.
- [39] G. Z. Li, G. G. Wang, Y. W. Cai, N. Sun, F. Li, H. L. Zhou, H. X. Zhao, X. N. Zhang, J. C. Han, Y. Yang, *Nano Energy* **2020**, *75*, 104918.
- [40] H. F. Qin, G. Q. Gu, W. Y. Shang, H. C. Luo, W. H. Zhang, P. Cui, B. Zhang, J. M. Guo, G. Cheng, Z. L. Du, *Nano Energy* **2020**, *68*, 104372.
- [41] W. Y. Shang, G. Q. Gu, W. H. Zhang, H. C. Luo, T. Y. Wang, B. Zhang, J. M. Guo, P. Cui, F. Yang, G. Cheng, Z. L. Du, *Nano Energy* **2021**, *82*, 105725.